CFD modelling of gas cell target for laser wakefield accelerators

Contact: runfeng.luo18@imperial.ac.uk

R. Luo, G. Christian, J. Hills, C. Cobo, E. Los, L. Kennedy, M. P. Backhouse, Z. Najmudin
The John Adams Institute
Imperial College London
SW7 2BZ, United Kingdom

N. Lopes
GoLP/Instituto de Plasmas e Fusão Nuclear
Instituto Superior Técnico
1049-001 Lisboa, Portugal

P. Blum, R. Shalloo
Deutsches Elektronen-Synchrotron DESY,
Notkestr. 85, 22607 Hamburg, Germany

E. Gerstmayr, J. Sarma, G. Sarri
School of Mathematics and Physics
Queen's University Belfast
BT7 1NN, United Kingdom

N. Bourgeois
Central Laser Facility
Rutherford Appleton Laboratory, Didcot
OX11 0QX, United Kingdom

Abstract

We performed 3D fluid simulations of a tunable length gas cell designed to vary in length between 0 cm and 5 cm. The simulations predict that the density non-uniformity inside the cell drops below 1% after 300 ms. We present a method to estimate the density equilibrium time based on the fluid simulations, which can be used to estimate the minimal delay for the initiation of gas flow to enable a uniform target density. This has implications for optimising electron beam quality and reproducibility in wakefield acceleration.

1 Introduction

Laser-wakefield acceleration (LWFA) is a novel type of accelerator that accelerates electrons to relativistic speeds by using a laser to drive a plasma wave. Typical targets are gas jets, gas cells and capillary discharge. Varying the target length is challenging for gas jets and capillary discharge. The length is typically set by the originally engineered design. A gas cell typically consists of an inlet and two outlets along the laser direction. Some gas cells adopt a movable piston [1]. This allows the gas cell to be adjusted between a few hundred micrometres up to a few centimetres.

The length control makes the gas cell suitable for a wide range of densities as the distance to reach the maximum electron energy scales inversely with density. Additionally, the variable cell length allows direct control of the electron energy by changing the acceleration distance. This allows the acceleration dynamics to be determined [14]. The outlets can be designed to tailor the shape of the density profile and the scale length of the density profile, which is important for optimising the LWFA electron beam quality. Furthermore, a homogeneous density inside the cell is critical for stability, as the laser evolution and the electron acceleration is strongly affected by the density. Density perturbations might introduce uncontrolled electron injection and also scatter already injected electrons, which can degrade the beam quality [3]. Gas cells provide more uniform density compared to gas jets which are subjected to small-scale plasma density gradients over a range of only a few plasma wavelengths, λ_p. This den-

sity non-uniformity causes fluctuations in the plasma wavelength, which is dependent on density. S. Kuschel et al. reported a gradient of $\partial_z \lambda_p = 3\%$ [8]. To model the density distribution inside the gas cell, computational fluid dynamics (CFD) simulations can be employed.

Many CFD solvers require fine-tuning of several parameters to achieve a stable solution. Artificial viscosity, for instance, is introduced to suppress numerical oscillations, especially when dealing with shocks. It is challenging for CFD solvers to simulate vacuum and extreme density changes [9]. Ryujin is an open-source finite-element solver for conservation equations such as the compressible Navier-Stokes and Euler equations of gas dynamics [6, 10]. The code uses a convex limiting algorithm to ensure a converging solution without the need for any tuning parameters. The robust numeric strategy guarantees convergence even under extreme shock conditions and complex geometries, making Ryujin particularly suitable for modelling scenarios with significant density variation, sharp transitions and real-life geometries such as gas cell setups.

2 Simulations

A tunable length gas cell designed for ionisation injection was simulated. The helium gas doped with a few percent of nitrogen by mass is fed into the cell for controlled ionisation injection [3, 11, 13]. The nitrogen K-shell electrons are only ionised near the peak laser intensity, where the laser pulse is strongest [12]. By adjusting the laser focus, the timing of the injection can be controlled to produce high-quality electron beams [15].

FIG. 1 is an illustration of the gas cell design. The target's length is defined as the distance between the piston tip and the outlet. A smooth on-axis density profile is desirable for high-quality electron beams. Therefore, the nozzle is designed with a convergent section, a throat, and a divergent section, similar to the de Laval nozzle used in rocket design [4]. This configuration smooths the transition from the subsonic flow to the supersonic flow, reducing abrupt density changes that degrade beam quality, and provides a long output scalelength to allow adiabatic damping of betatron motion [2].

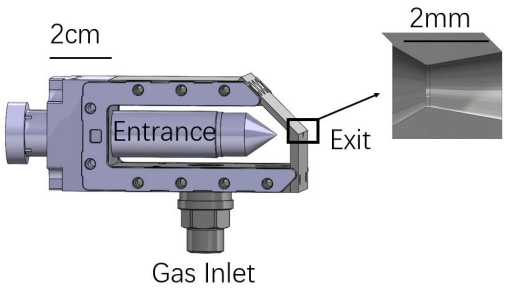

Figure 1: Drawing of the cell geometry and a zoomed-in plot of nozzle at the laser exit.

To investigate the sonic and supersonic flows that can occur in the gas cell, an optimised solver module for the compressible Euler equations was used. Ryujin's convex limiting algorithm ensures the preservation of key physical invariants by enforcing entropy inequalities. This convex limiting scheme characterises shocks and discontinuities without the need for artificial tuning parameters, unlike other schemes that might become questionable for supersonic and transonic flows due to the lack of pointwise stability.

We simulated pure helium with an inlet pressure of 100 mbar. The density was calculated from the ideal gas law, assuming the temperature was 300 K. The initial vacuum pressure was assumed to be 10^{-5} mbar. It is worth noting that the wall conditions were set to slip. The Knudsen number, Kn, is the ratio of the molecular mean free path to the physical scale in the system. It characterises the type of the flow. For $Kn < 0.01$, the continuum flow assumption is valid, and the no-slip boundary condition applies. For $0.01 < Kn < 0.1$, the velocity slip at the wall becomes important, and the slip boundary conditions should be used [17]. The Knudsen number for helium at 300 K and 100 mbar, with the nozzle throat as the smallest length scale at 20 µm is approximately 0.069. This value indicates that the gas flow in the cell

is within the transitional regime, between continuum flow and free molecular flow, where rarefied gas effects start to emerge.

3 Results

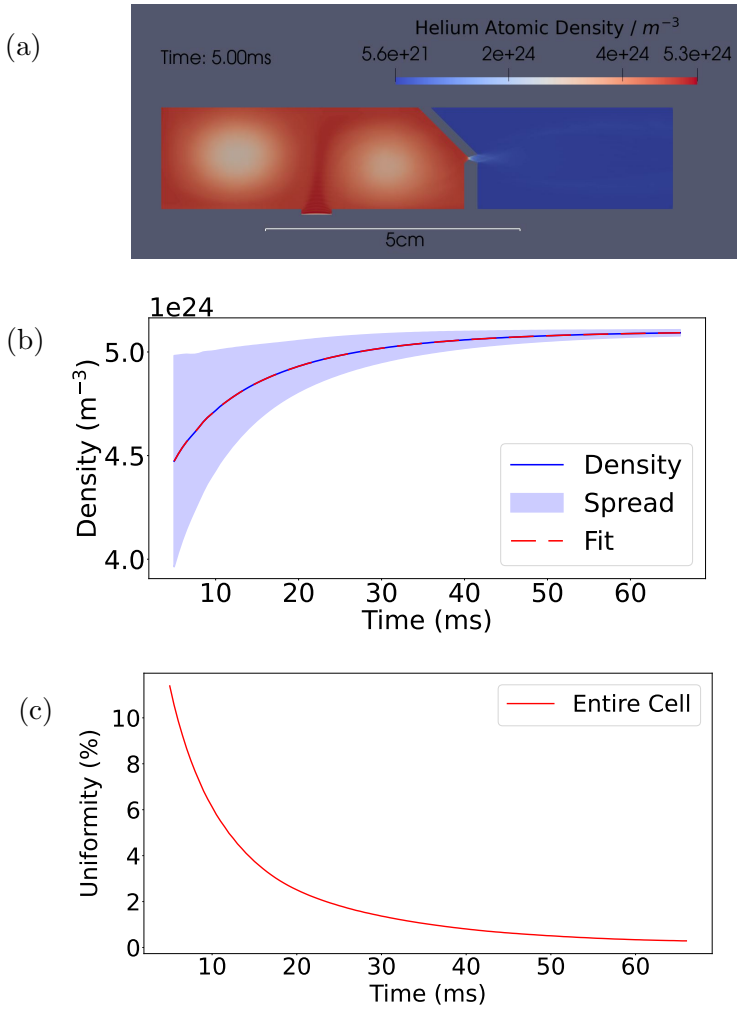

Figure 2: Density distribution and density uniformity for the simplified 2D geometry. (a) A transverse slice of the density distribution at 5 ms. (b) Mean helium atomic density in the entire cell. (c) Density uniformity.

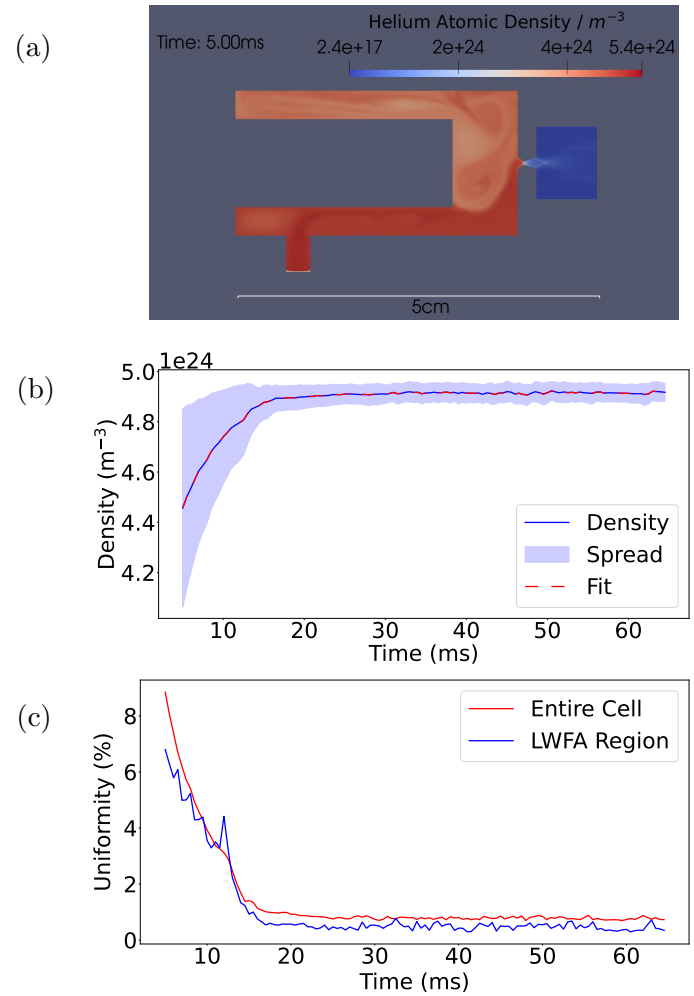

Figure 3: Density distribution and density uniformity for the 2D cell geometry. (a) A transverse slice of the density distribution at 5 ms. (b) Mean helium atomic density in the entire cell. (c) Density uniformity.

The density equilibrium time of a gas cell sets the minimum time for the delay, before which the laser can be fired into the cell. After this delay, the cell can be considered sufficiently uniform to facilitate the production of a high-quality electron beam. The characteristic time scale, τ, is the time constant for the exponential increase in cell density.. The density requires approximately two to three characteristic times to achieve uniformity within 1%, measured as the standard deviation (s.t.d.) of the density inside the cell. The characteristic time can be estimated as the ratio of the fluid mass contained within the cell to the mass flow rate exiting through the nozzle. τ is given by [5]:

$$\tau = \frac{V}{C_d A_{outlet}} \sqrt{\frac{\rho_0}{2\Delta P}}, \qquad (1)$$

where ρ_0 is the density, and ΔP is the pressure difference between the cell and the vacuum. C_d is the discharge coefficient, which is close to

unity for a nozzle [16]. A_{outlet} is the area of the outlet, and V is the volume of the cell. The ratio of the volume of the cell to the size of the outlet is dependent on the dimensionality of the simulation. It can be shown that,

$$\tau_{3d} = \tau_{2d} \frac{2L_{cell}}{\pi r_{outlet}} \tag{2}$$

L_{cell} is the length of the cell in the direction perpendicular to the plane of the 2D simulation, and r_{outlet} is the radius of the outlet. Therefore, τ_{3d} is approximately 25.5 times longer than τ_{2d}.

To test the capability of the Ryujin code, we performed 2D trial simulations with a simplified geometry, as shown in FIG. 2a). The density plateaus at $5.09 \times 10^{25}\,\mathrm{m}^{-3}$ after 50 ms. The mean density in the cell exhibited an exponential increase with a characteristic time of 11.5 ms. FIG. 3 shows the results for the 2D simulation with a more realistic representation of the gas cell. This model includes a plunger mechanism that enables adjustment of the gas cell length. Flows around the plunger might introduce density inhomogeneities that are not accounted for in the simplified model lacking the plunger. FIG. 3a) is an illustration of the cell geometry. The cell consists of an inlet at the bottom and a piston inside. The outlet on the piston was neglected, as the area is much smaller as compared to the nozzle size. We observe that the density levels off at $4.92 \times 10^{25}\,\mathrm{m}^{-3}$ after 30 ms. The small density deviation from the 2D simplified geometry is caused by the different vacuum and cell geometries. The mean density showed an exponential increase with a characteristic time of 4.92 ms. The density inhomogeneity in both the entire cell and the LWFA region, defined as a cylinder within the cell with a radius twice that of the outlet and centered along the laser direction, decreased to below 1% after 20 ms. The piston reduces the volume inside the cell, which leads to a smaller characteristic time. This is consistent with Eq. 1.

The 2D simulations are fast to compute, but to investigate the full 3D behavior, we conducted 3D simulations that require significantly longer computational times. The simulations were performed on the Imperial HPC system with 4 nodes and 64 Icelake CPUs on each node [7]. The 2D simulations only took a few hours to run. In comparison, it took eight days to compute 400 ms for the 3D simulation. FIG. 4 illustrates the gas cell geometry for the 3D simulation, and FIG. 5 shows the mean density inside the cell plateaus after 400 ms. The characteristic time is about 100 ms for the mean density increase. The density spread in the cell decreases to below 1% after 300 ms.

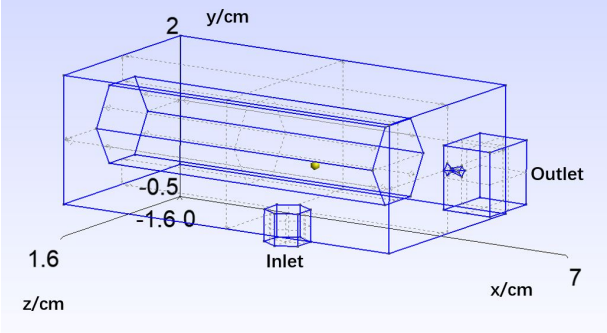

Figure 4: View of the cell geometry used for 3D simulations.

The equilibrium time is much longer than the 2D case. The longer equilibrium time is caused by the fact that there is a larger volume to fill in 3D, which agrees with Eq. 1. FIG. 5c) compares the density spread in the entire cell and in the LWFA region. There is a smaller density spread in the LWFA region. After the initial fluctuations, the density spread decreases monotonically after 220 ms, reaching 0.165% at 400 ms. For LWFA operation, the laser can be fired once the density in the interaction region becomes uniform.

4 Conclusion

We performed 2D and 3D simulations of the variable gas system. A standard deviation of the density below 1% was observed for both 2D and 3D simulations. The high density uniformity reduces shot-to-shot instabilities caused by density fluctuations. This demonstrates that a gas cell target provides much finer control over density compared to a gas jet. We have shown

(a)

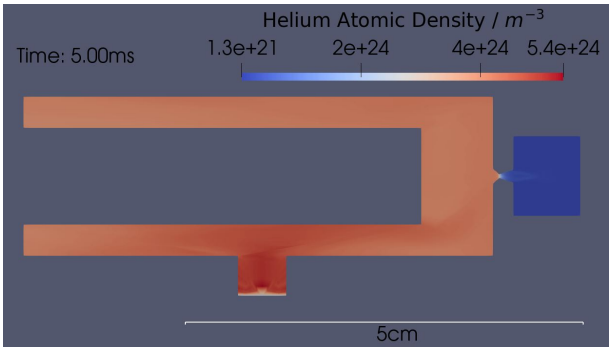

(b)

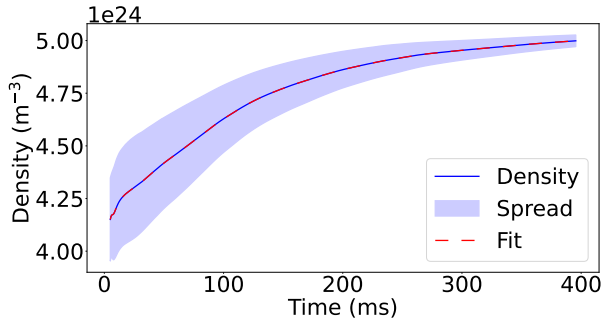

(c)

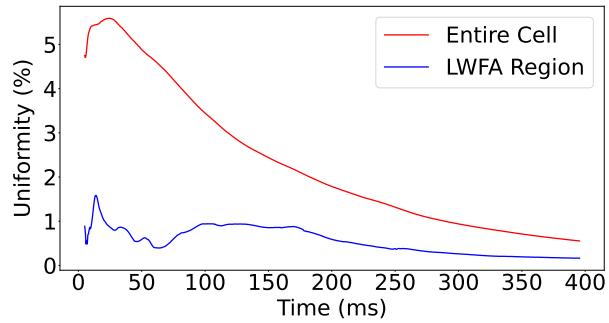

Figure 5: Density distribution and density spread for the 3D cell geometry. a) A transverse slice of the density distribution at 5 ms. b) Mean helium atomic density. c) Density uniformity.

that the 2D simulations underestimate the true equilibrium time, and 3D simulations should be employed to estimate the time it takes for the gas to settle inside the cell. The 3D simulation shows a characteristic time of 110 ms for a gas cell with a volume of 38 cm^3, and predicted that the density variation inside the cell drops below 1% after 300 ms. The results predict the appropriate interval between the gas release time and when the laser arrives, which has implications for high-quality electron beams. The long equilibrium suggests that a gas cell in pulsed mode will not be suitable for high-repetition-rate LWFA. For a 10 Hz LWFA, a gas cell in continuous mode might provide a more uniform density profile.

The authors acknowledge funding from STFC (ST/J002062/1, ST/P002021/1, ST/V001639/1), and support from the Imperial College Research Computing Service.

References

[1] C. Aniculaesei, Hyung Taek Kim, Byung Ju Yoo, Kyung Hwan Oh, and Chang Hee Nam. Novel gas target for laser wakefield accelerators. *Review of Scientific Instruments*, 89, 2018.

[2] Michael Backhouse. *Measurement and optimisation of beam quality from laser wakefield accelerators*. PhD thesis, Imperial Coll., London, 2022.

[3] Simon Bohlen, Jonathan C. Wood, Theresa Brümmer, Florian Grüner, Carl A. Lindstrøm, Martin Meisel, Theresa Staufer, Richard D'Arcy, Kristjan Põder, and Jens Osterhoff. Stability of ionization-injection-based laser-plasma accelerators. *Physical Review Accelerators and Beams*, 25, 2022.

[4] Nikhil D Deshpande, Suyash S Vidwans, Pratik R Mahale, Rutuja S Joshi, and K R Jagtap. Theoretical CFD analysis of De Laval nozzle. *4th IRF International Conference*, 5, 2014.

[5] Anna Golijanek-Jedrzejczyk, Dariusz Świsulski, Robert Hanus, Marcin Zych, and Leszek Petryka. Uncertainty of the liquid mass flow measurement using the orifice plate. *Flow Measurement and Instrumentation*, 62, 2018.

[6] Jean-Luc Guermond, Martin Kronbichler, Matthias Maier, Bojan Popov, and Ignacio Tomas. On the implementation of a robust and efficient finite element-based parallel solver for the compressible Navier-Stokes equations. *Computer Methods in Applied*

Mechanics and Engineering, 389:114250, 2022.

[7] Imperial College Research Computing Service. Imperial College Research Computing Service. Accessed: 2024-09-06.

[8] S. Kuschel, M. B. Schwab, M. Yeung, D. Hollatz, A. Seidel, W. Ziegler, A. Sävert, M. C. Kaluza, and M. Zepf. Controlling the self-injection threshold in laser wakefield accelerators. *Physical Review Letters*, 121, 2018.

[9] C. Liu, G. Zhou, W. Shyy, and K. Xu. Limitation principle for computational fluid dynamics. *Shock Waves*, 29, 2019.

[10] Matthias Maier and Martin Kronbichler. Efficient parallel 3d computation of the compressible Euler equations with an invariant-domain preserving second-order finite-element scheme. *ACM Transactions on Parallel Computing*, 8(3):16:1–30, 2021.

[11] C. McGuffey, A. G.R. Thomas, W. Schumaker, T. Matsuoka, V. Chvykov, F. J. Dollar, G. Kalintchenko, V. Yanovsky, A. Maksimchuk, K. Krushelnick, V. Yu Bychenkov, I. V. Glazyrin, and A. V. Karpeev. Ionization induced trapping in a laser wakefield accelerator. *Physical Review Letters*, 104, 2010.

[12] A. Pak, K. A. Marsh, S. F. Martins, W. Lu, W. B. Mori, and C. Joshi. Injection and trapping of tunnel-ionized electrons into laser-produced wakes. *Physical Review Letters*, 104, 2010.

[13] T. P. Rowlands-Rees, C. Kamperidis, S. Kneip, A. J. Gonsalves, S. P.D. Mangles, J. G. Gallacher, E. Brunetti, T. Ibbotson, C. D. Murphy, P. S. Foster, M. J.V. Streeter, F. Budde, P. A. Norreys, D. A. Jaroszynski, K. Krushelnick, Z. Najmudin, and S. M. Hooker. Laser-driven acceleration of electrons in a partially ionized plasma channel. *Physical Review Letters*, 100, 2008.

[14] A. Sävert, S. P.D. Mangles, M. Schnell, E. Siminos, J. M. Cole, M. Leier, M. Reuter, M. B. Schwab, M. Möller, K. Poder, O. Jäckel, G. G. Paulus, C. Spielmann, S. Skupin, Z. Najmudin, and M. C. Kaluza. Direct observation of the injection dynamics of a laser wakefield accelerator using few-femtosecond shadowgraphy. *Physical Review Letters*, 115, 2015.

[15] Jinguang Wang, Jie Feng, Changqing Zhu, Yifei Li, Yuhang He, Dazhang Li, Junhao Tan, Jinglong Ma, and Liming Chen. Small energy spread electron beams from laser wakefield acceleration by self-evolved ionization injection. *Plasma Physics and Controlled Fusion*, 60, 2018.

[16] J.L. Woodward. Source modeling – discharge rates. In *Reference Module in Chemistry, Molecular Sciences and Chemical Engineering*. Elsevier, 2014.

[17] Liehui Zhang, Shan Baochao, Zhao Yulong, and Guo Zhaoli. Review of micro seepage mechanisms in shale gas reservoirs, 2019.